J Mater Sci (2021) 56:14257–14269

Materials for life sciences

Exploring hierarchical porous silica-supported Ag_3PO_4 as high-efficient and environmental-friendly photocatalytic disinfectant

Pei Zheng[1,2,*], Bo Jin[2], and Sheng Dai[3,*]

[1] College of Geography and Environment, Baoji University of Arts and Sciences, Baoji 721013, China
[2] School of Chemical Engineering, The University of Adelaide, Adelaide, SA 5005, Australia
[3] Department of Chemical Engineering, Brunel University London, Uxbridge UB8 2DW, UK

Received: 7 December 2020
Accepted: 27 January 2021
Published online: 1 June 2021

ABSTRACT

Silver orthophosphate (Ag_3PO_4) is an attractive photocatalytic catalyst for disinfection and degradation, but its instability arising from silver release generates significant environmental issue. Aiming to develop a highly efficient and environmental-friendly catalyst, we synthesized Ag_3PO_4 nanoparticle incorporated hierarchical porous silica (Ag_3PO_4@*h*-SiO_2) as a novel high-performance photocatalytic catalyst without observed silver release. Brain-like hierarchical porous SiO_2 (*h*-SiO_2) brings a scaffold support with high surface areas, and the *h*-SiO_2 surface modified thiols are able to anchor in situ formed 10 nm Ag_3PO_4 to eliminate silver release. Systematic investigations revealed that because of its structural advantages, Ag_3PO_4@*h*-SiO_2 show excellent disinfection and degradation ability under visible-light irradiation and stable characteristics without obviously observed silver leaching during photo-oxidation operation. In-depth scavenger study reveals Ag_3PO_4@*h*-SiO_2 as an effective semiconducting photocatalyst stimulates the production of photo-generated reactive species, which dominate its distinguished disinfection performance via photo-oxidation.

Handling Editor: Maude Jimenez.

Address correspondence to E-mail: pei.zheng@hotmail.com; sheng.dai@brunel.ac.uk

https://doi.org/10.1007/s10853-021-05852-y

GRAPHICAL ABSTRACT

Ag_3PO_4 are anchored to thiol modified hierarchical porous SiO_2 to produce a visible-light responsive photocatalyst of Ag_3PO_4@h-SiO_2. The enhanced catalytic sites and surface areas promote pathogen disinfection, and the structure advantages minimize silver release to environment. Both H_2O_2 and holes being generated in photocatalysis dominate overall disinfection activity.

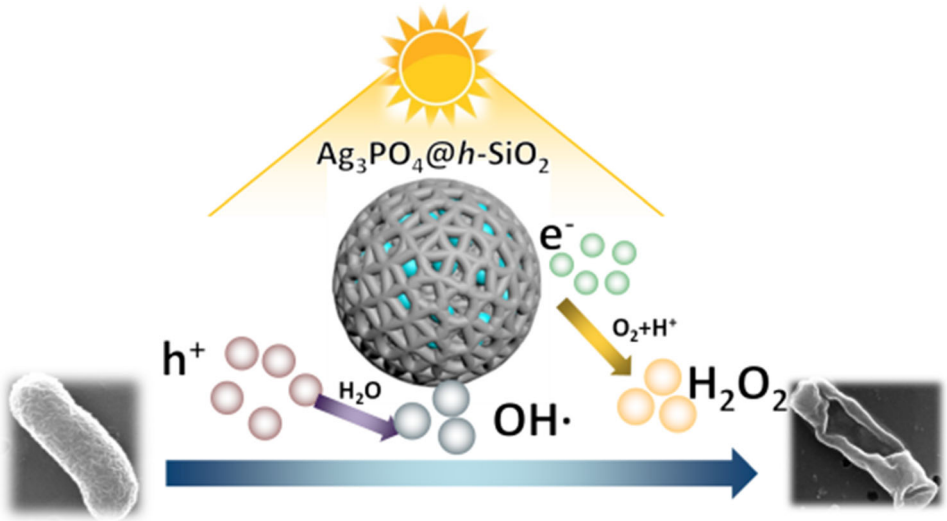

Introduction

The growing concern about potential health risk caused by the arising of multidrug-resistant pathogenic microorganisms and increasing occurrences of cross-microbial contamination have put more stress on the development of high efficient disinfectants [1–3]. Conventional disinfectants like detergents, alcohols and chlorine chemicals are not environmental-friendly and inefficient for long-term application [4]. Semiconductor-mediated heterogeneous photocatalytic materials have been considered as promising alternatives since Matsunaga first reported the disinfection of platinum-doped TiO_2 mediated photo-catalysis in 1985 [1, 2]. The reactive oxygen species (ROS) and photo-generated holes can non-selectively destruct a wide range of microbial species and organics in solution [3]. To date, the disinfection of varied semiconductor-based photocatalysts such as TiO_2, ZnO, CdS and ZnS have been widely studied [4–7]. However, their performance and capabilities in utilizing UV region limited their practical use [8]. Thus, the development of broad-spectrum photocatalysts including visible range as new disinfectants is of significance and challenge.

Recently, silver orthophosphate (Ag_3PO_4) semiconductor has been reported to exhibit exceedingly great photo-oxidative performance under visible-light irradiation for oxidizing water and decomposing organic contaminant, significantly higher than commercial $TiO_{2-x}N_x$ [9]. However, there are some inherent shortcomings of Ag_3PO_4 as an ideal photocatalytic replacement disinfectant. Without a physical support, Ag_3PO_4 NPs tend to aggregate in solution which not only causes deterioration of their physicochemical properties and difficulty to recycle but also decreases their disinfection performance and gradually diminishes their disinfection efficacy after long-term operation [10, 11]. On the other hand, instability of Ag_3PO_4 leads to silver leaching, resulting in reduced disinfection capability and significant environmental risk [8, 12]. Therefore, Ag_3PO_4 immobilization and silver release control are crucial to

explore it as an effective photocatalyst in a continuous disinfection operation. Till now, several practices have been explored as the support to anchor or immobilize Ag_3PO_4, such as CNTs, graphene, SiO_2 and hydroxyapatite (HA) [8, 12–18]. CNTs and graphene are expensive, and HA has a propensity for biofilm formation. Silica is an excellent support candidate due to its low cost, easy preparation, good biocompatibility, materials inertness and easy surface modification [12, 19–21]. Although some preliminary studies have reported the deposition of Ag_3PO_4 onto SiO_2 spheres, Ag_3PO_4 aggregation and silver release still remain challenging [15, 16, 18, 22].

Inspired by our research on exploring hierarchical porous silica for biopharmaceutical applications [23–25], we here develop a facile in situ precipitation approach to load 10 nm Ag_3PO_4 NPs onto the thiol modified hierarchical porous silica to generate the Ag_3PO_4@*h*-SiO_2 and investigate their photocatalytic disinfection performance. Such a unique structure possesses obvious advantages of high specific surface areas, high Ag_3PO_4 loading, reduced Ag_3PO_4 aggregation, better chemical and physical durability. From systematic studies, Ag_3PO_4@*h*-SiO_2 exhibits enhanced photocatalytic disinfection performance over bulk Ag_3PO_4 under visible-light irradiation and there is no obviously observed silver leaching. The disinfection performance trends towards the reactive oxygen species generated from visible-light induced photocatalytic chemistry.

Experimental section

Material

Tetraethyl orthosilicate (TEOS), triethanolamine (TEA), cetyltrimethylammonium *p*-toluenesulfonate (CTAT), 3-mercaptopropyltrimethoxysilane (MPTMS) and other chemicals were supplied by Sigma-Aldrich and used without any purification. De-ionized (DI) water was used though all experiments. *E. coli* was provided by the University of Adelaide.

Preparation of Ag_3PO_4@h-SiO_2 nanoparticles

h-SiO_2 NPs were synthesized through a soft-templating method with slight modification using TEOS as silica precursor, TEA as base catalyst, CTAT as structure-directing agent [20, 24]. Typically, 0.48 g CTAT and 0.087 g TEA were dissolved in 25 mL DI water (80 °C). 3.9 mL TEOS was then quickly added into the above mixture and refluxed for 2 h. White precipitates were collected by centrifugation and washed with DI water and then dried at 60 °C overnight. After that, surfactant templates were removed by calcination in air at 700 °C for 3 h at a ramp rate of 2 °C min^{-1} to obtain the hierarchical silica.

h-SiO_2 surface modification with thiols (HS-*h*-SiO_2) was achieved by grafting MPTMS onto the above-prepared hierarchical silica [21]. 0.1 g h-SiO_2 was added into 2.5 ml n-hexane containing 0.2 g MPTMS, agitated for 18 h, centrifuged and then washed with absolute ethanol for three times.

Deposition of Ag_3PO_4 to the surface-functionalized *h*-SiO_2 was conducted using an *in situ* precipitation method. Briefly, HS-*h*-SiO_2 was dispersed in 10 mL $AgNO_3$ aqueous solution (1.8 mM). Then, the dispersion was agitated for 24 h at room temperature, allowing adsorption equilibrium. The silver ion saturated HS-*h*-SiO_2 was then filtered and re-suspended in 10 ml DI water. After that, 20 mL Na_2HPO_4 aqueous solution (0.6 mM) was added slowly, refluxed 3 h. Precipitates were collected, washed with DI water and ethanol and then dried overnight to obtain the Ag_3PO_4@*h*-SiO_2. Bulk Ag_3PO_4 NPs were synthesized using the same way without adding HS-*h*-SiO_2.

10 mg Ag_3PO_4@*h*-SiO_2 was dissolved in 5% HNO_3 for ICP-MS measurement, and actual Ag weight percentage was determined to be 11.07% (i.e. Ag_3PO_4 weight percentage of 15.82%) in Ag_3PO_4@*h*-SiO_2.

Characterization

To better understand the prepared NPs, their morphology and structural analysis were studied by scanning electron microscopy (SEM), energy-dispersive X-ray (EDX), X-ray diffraction (XRD), and UV–vis. The sizes and specific surface areas were also investigated by dynamic light scattering (DLS) and Brunauer−Emmett–Teller (BET) methods.

Photocatalytic degradation of organics

To study the photocatalytic efficiencies of the prepared Ag_3PO_4@*h*-SiO_2, *h*-SiO_2 and Ag_3PO_4 NPs, methylene blue (MB) degradations were studied

under visible-light irradiation with different nanoparticle dosages (0.010 g Ag_3PO_4@*h*-SiO_2, 0.0085 g h-SiO_2 and 0.0015 g Ag_3PO_4) dispersed in MB solution (20 mL, 15 μM) under vigorous agitation. All suspensions were firstly agitated in dark for 45 min to reach adsorption/desorption equilibrium before introducing light source. A 300 W Xe arc lamp (PerfectLight, PLS-SXE300C, Beijing) equipped with a UV cutoff filter (UVCUT420, $\lambda > 420$ nm) was used as the light source, which was located 20 cm from reaction solutions. To monitor the MB concentration change during the experiments, a specific amount of the suspension was collected at a set frequency, centrifuged and measured by using a UV–Vis spectrophotometer.

Disinfection evaluation

Escherichia coli was selected as a model pathogen to test disinfection efficiencies of the synthesized NPs. A chloride ion-free buffer solution was prepared and used through the whole disinfect experiments [18]. E.coli was first cultured to yield a suspension with viable cell density of about 10^9 CFU mL^{-1} [18]. Then, designed dosages of Ag_3PO_4@*h*-SiO_2 (2.0 mg), *h*-SiO_2 (1.7 mg) and Ag_3PO_4 (0.3 mg) were separately added into 20 mL of the above *E coli* suspension. During the experiment, the suspensions were agitated gently at room temperature and irradiated by visible light. At set time intervals, 0.1 ml aliquots were plated on agar plates. The viable *E coli* colonies were counted after those plates were incubated at 37 °C overnight. For comparison, dark control experiments without light irradiation and blank control in the absence of any NPs were performed. All experiments were carried out in triplicates. Kirby–Bauer method was also performed to compare the disinfection abilities of the synthesized NPs in a quantitative and visual way. The chosen pathogen was spread evenly on agar plates covered with small round filter disks carrying little volume (10 μL) of buffer solution and NP suspensions. Those agar plates were left in dark/ visible light for 10 min and then incubated overnight at 37 °C for observation.

Shape analysis of E. coli

The morphological change of *E. coli* before and after Ag_3PO_4@*h*-SiO_2 photo-disinfectant treatment was monitored by SEM. The bacteria (10^9 CFU mL^{-1}) were inoculated in sterilized buffer solution containing 0.1 mg/mL Ag_3PO_4@*h*-SiO_2. The mixture was then irradiated under visible light for 50 min. After filtration, the critical point drying method was used to keep *E. coli* morphology [8, 18], and then observed using SEM technology.

Results and discussion

Synthesis and characterization of photocatalytic nanoparticles

The preparation of Ag_3PO_4@*h*-SiO_2 is schematically illustrated in Scheme 1. First, monodisperse hierarchical porous silica nanoparticles were synthesized through a soft-templating method [19]. *h*-SiO_2 nanoparticles were further surface functionalized with thiols by a post-synthesis grafting method. Silver ions were then loaded to thiols, and subsequently reacted with HPO_4^{2-} to in situ form Ag_3PO_4 nanocrystals inside the pores of *h*-SiO_2.

Morphologies of these NPs were examined by SEM and TEM. Figure 1a indicates that *h*-SiO_2 exhibits a brain-like spherical morphology with large pores and wrinkled surfaces. *h*-SiO_2 NPs have a uniform particle size of ~ 120 nm (Figure S1, SI) together with good dispersity in solution. TEM image (Fig. 1b) confirms the existence of hierarchical structures in *h*-SiO_2 NPs. Figure 1c shows that the Ag_3PO_4@*h*-SiO_2 well maintains the wrinkled surface, porous structure and good stability. The large specific surface area and hierarchical porous structure of Ag_3PO_4@*h*-SiO_2 provide promising microenvironment beneficial for molecular interfacial reaction, molecular adsorption capacity, photocatalytic kinetics and consequently photo-disinfection ability. The identical particle sizes of Ag_3PO_4@*h*-SiO_2 and *h*-SiO_2 (Figure S1, SI) indicate the presence of Ag_3PO_4 NPs inside the pores of *h*-SiO_2 rather than on surface. TEM image of Ag_3PO_4@*h*-SiO_2 (Fig. 1d) clearly depicts that Ag_3PO_4 are well scattered in the large pores of *h*-SiO_2 with an average size of ~ 10 nm, which is much smaller than bulk Ag_3PO_4 NPs being prepared in the absence of *h*-SiO_2 (Figure S2, SI). Moreover, due to the presence of thiols on *h*-SiO_2 surface, Ag_3PO_4 can be stably chelated in the pores of *h*-SiO_2. Elemental analysis was studied by EDX (Figure S3, SI), where oxygen and silicon peaks come from *h*-SiO_2. Besides, the

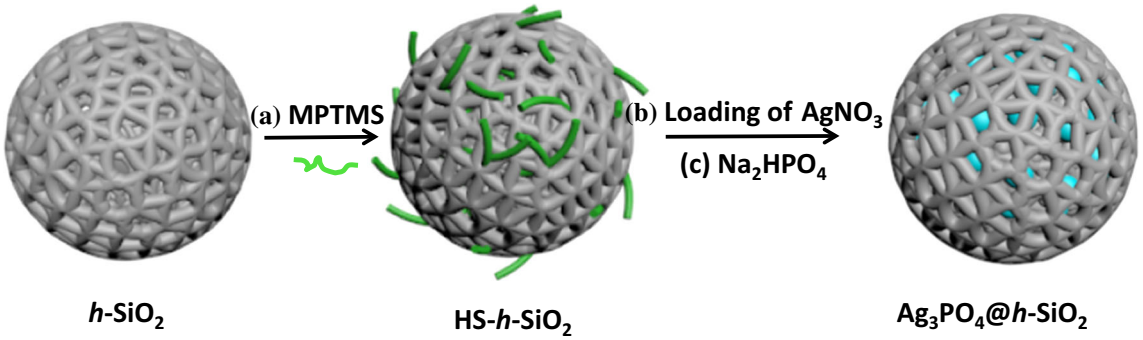

Scheme 1 Schematic illustration on the synthesis of Ag_3PO_4@*h*-SiO_2, where green bars represent –SH moieties and blue spheres represent Ag_3PO_4 NPs.

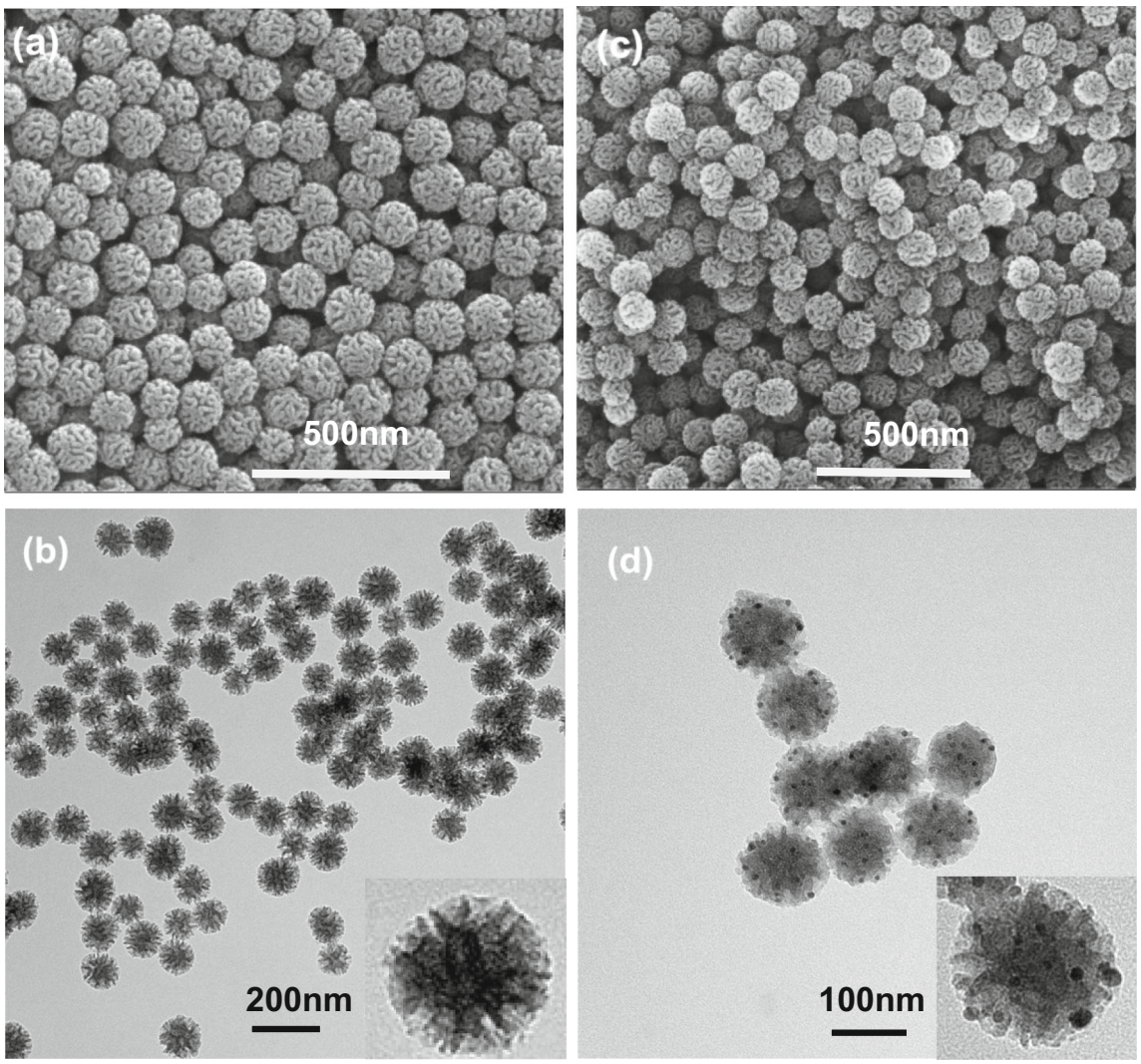

Figure 1 SEM and TEM images of *h*-SiO_2 **a**, **b** and Ag_3PO_4@*h*-SiO_2 **c**, **d**.

observation of Ag and P peaks confirms the formation of Ag_3PO_4@*h*-SiO_2.

The crystallographic analysis of the *h*-SiO_2, Ag_3PO_4 and Ag_3PO_4@*h*-SiO_2 was examined by XRD (Fig. 2). All diffraction peaks of pristine Ag_3PO_4 can be

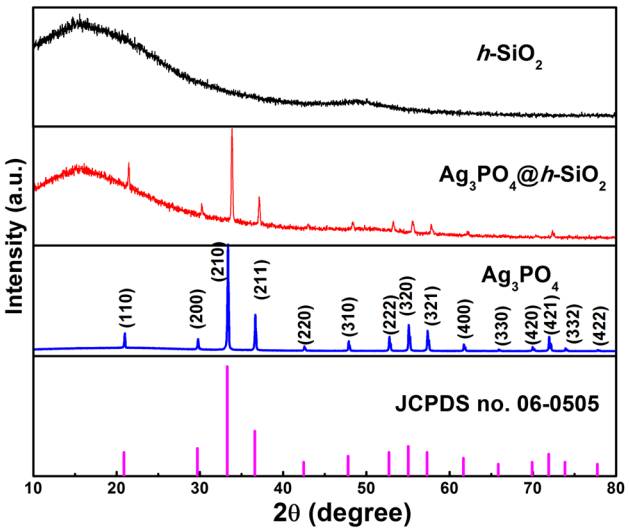

Figure 2 XRD patterns of h-SiO_2, Ag_3PO_4 and Ag_3PO_4@h-SiO_2.

indexed with the body-centered cubic (BCC) structure, which agree well with the JCPDS card no. 06–0505 [26]. In addition, it has been observed that the diffraction peaks for pristine Ag_3PO_4 and amorphous h-SiO_2 are well presented in the XRD pattern of Ag_3PO_4@h-SiO_2, confirming the successful preparation of h-SiO_2@Ag_3PO_4.

The UV–Vis study of the h-SiO_2, Ag_3PO_4 and Ag_3PO_4@h-SiO_2 has been presented in Figure S4 (SI). Bulk Ag_3PO_4 shows an apparent visible-light absorption band [26, 27]. h-SiO_2 exhibits no visible-light response because of its broad band gap of ~ 9 eV [28]. However, Ag_3PO_4@h-SiO_2 exhibits obvious visible-light absorbance, implying it is a potential visible-light inducing photocatalyst.

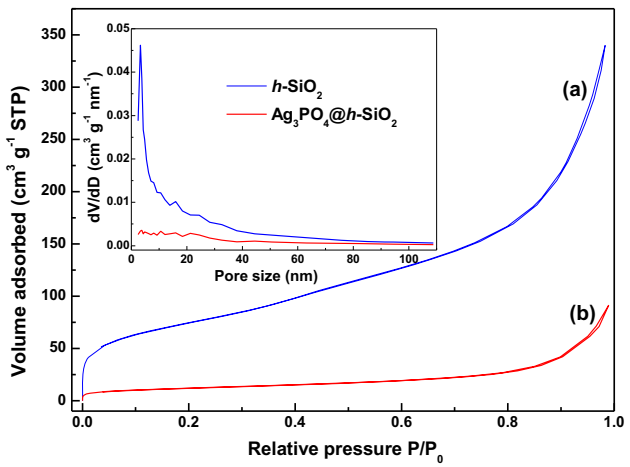

Figure 3 Nitrogen adsorption–desorption isotherms and pore size distributions of **a** h-SiO_2 and **b** Ag_3PO_4@h-SiO_2.

Nitrogen adsorption–desorption isotherms and pore size distributions (PSD) of h-SiO_2 and Ag_3PO_4@h-SiO_2 show type-IV isotherms with narrow hysteresis loops (Fig. 3) [29]. The BET surface areas of h-SiO_2 and Ag_3PO_4@h-SiO_2 are calculated to be 254 and 40 m^2g^{-1}. The decrease in pore volume from 0.489 for h-SiO_2 to 0.135 cm^3g^{-1} for Ag_3PO_4@h-SiO_2 confirms that Ag_3PO_4 have been loaded to the pores of h-SiO_2. The size of loaded Ag_3PO_4 NPs of about 10 nm is much smaller than that being prepared in bulk (Figure S2, SI), and smaller Ag_3PO_4 NPs may provide larger specific surface areas, beneficial for enhancing its photocatalytic disinfection performance.

Photocatalytic degradation of organics

Photocatalytic efficiencies of the Ag_3PO_4@h-SiO_2 were preliminarily studied by degrading a model organic dye methylene blue (MB) under visible-light irradiation (Fig. 4). From the ICP-MS results, the silver content in Ag_3PO_4@h-SiO_2 is ~ 11 wt%, i.e. there is ~ 15 wt% of Ag_3PO_4 and ~ 85 wt% of h-SiO_2 in the Ag_3PO_4@h-SiO_2. In the systematic photocatalytic evaluation, comparable dosages of Ag_3PO_4@h-SiO_2 (0.5 mg/mL), h-SiO_2 (0.425 mg/mL, 85 wt% of Ag_3PO_4@h-SiO_2) and Ag_3PO_4 (0.075 mg/mL, 15 wt% of Ag_3PO_4@h-SiO_2) were used for MB degradation. Blank control experiments were conducted as a reference. All suspensions were agitated in dark for

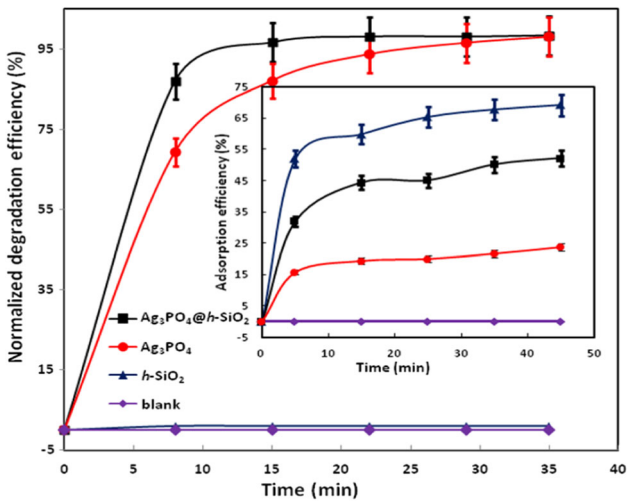

Figure 4 Photocatalytic degradation of MB (20 mL, 15 μM) under visible-light irradiation at room temperature and adsorptive performance of h-SiO_2 (0.425 mg/ml), Ag_3PO_4 (0.075 mg/ml) and Ag_3PO_4@h-SiO_2 (0.5 mg/ml) shown as the inset.

45 min to achieve adsorption/desorption equilibrium before visible light was introduced (Fig. 4, inset). *h*-SiO_2 achieves the highest MB adsorption (~ 69.2%) compared to Ag_3PO_4@*h*-SiO_2 (~ 52.2%) and bulk Ag_3PO_4 (~ 23.7%), which can be attributed to their different specific surface areas. Beyond the adsorption/desorption equilibrium, photocatalytic experiments of MB degradation were initiated by introducing visible light. After 35 min of visible-light irradiation, there was no change for MB alone, showing MB cannot be remarkably degraded by visible light. Similarly, MB was not degraded in the presence of *h*-SiO_2, which can be ascribed to its low responsiveness to visible light. Using bulk Ag_3PO_4, MB can be degraded completely within 35 min. It is notable that only 15 min is required to achieve complete MB degradation using the Ag_3PO_4@*h*-SiO_2 under same experimental condition. These enhanced photocatalytic MB degradation of Ag_3PO_4@*h*-SiO_2 is attributed by its superior structure advantage, where the hierarchical structures of Ag_3PO_4@*h*-SiO_2 facilitate MB physical adsorption and interfacial photocatalytic degradation associated with its high porosities and large surface areas.

Disinfection evaluation

The disinfection performance of Ag_3PO_4@*h*-SiO_2 as a photocatalyst was investigated using *E. coli* as a representative pathogen. To avoid protein adsorption and AgCl precipitation, all disinfection evaluations were conducted in chlorine-free buffer media [4, 18]. Prior to experiments, *E. coli* were thoroughly washed and re-suspended in chlorine-free buffer solution.

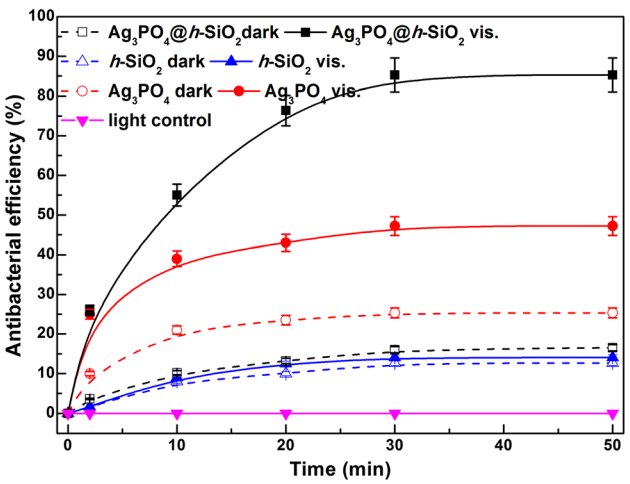

Figure 5 Disinfection profiles against *E. coli* (10^9 CFU ml^{-1}): 85 μg/ml *h*-SiO_2 in dark (Triangle) and under visible-light irradiation (Filled Triangle); 15 μg/ml Ag_3PO_4 in dark (Circle) and under visible-light irradiation (Filled Circle); 100 μg/ml Ag_3PO_4@*h*-SiO_2 in dark (Square) and under visible-light irradiation (Filled Square).

Like previous MB photocatalytic experiment, comparable dosages of Ag_3PO_4@*h*-SiO_2 (100 μg/mL), *h*-SiO_2 (85 μg/mL, ~ 85% of Ag_3PO_4@*h*-SiO_2) and Ag_3PO_4 (15 μg/mL, 15% of Ag_3PO_4@*h*-SiO_2) were used in disinfection tests at room temperature. Figure 5 shows the *E. coli* disinfection profiles for the above NPs under visible-light irradiation. As references, dark controls were performed under the same NP dosages without illumination, and blank control was carried out under visible-light irradiation but without adding any NPs. Like MB degradation, visible-light irradiation does not display any disinfection activity without NPs. Due to its poor response to visible light, *h*-SiO_2 shows identical 15.2% disinfection over 50 min under both illumination and dark conditions. Slight SiO_2 toxicity to both *E. coli* and *B. subtilis* under both light and dark conditions has been reported by Laura [30], and it also conforms with its low photocatalytic ability on MB degradation. Experimental data show that 47.2% *E. coli* are killed by bulk Ag_3PO_4 under 50 min visible-light irradiation, while 25.3% *E. coli* death in the dark control. Ag_3PO_4 has a BCC structure and low solubility in water [8, 13, 26], and the released silver can kill bacteria. [31, 32] Thus, the dark killing of bulk Ag_3PO_4 is mainly due to released silver [8, 12], while its enhanced disinfection activity under visible-light illumination is ascribed to its additional visible-light-driven photocatalytic ability [9, 33], 34. Therefore, both photo-responsiveness and sliver release dominate the overall disinfection of bulk Ag_3NO_4.

Figure 5 reveals the remarkable disinfection performance of Ag_3PO_4@*h*-SiO_2, where ~ 85.3% disinfectant efficiency can be achieved in 50 min visible-light irradiation by adding 0.1 mg/mL of Ag_3PO_4@*h*-SiO_2. At a comparable dosage of NPs, Ag_3PO_4@*h*-SiO_2 shows approximately double disinfection efficiency over bulk Ag_3PO_4 under 30 min visible-light irradiation. Interestingly, the Ag_3PO_4@*h*-SiO_2 demonstrates much lower disinfection efficiency in dark than bulk Ag_3PO_4. These results indicate that Ag_3PO_4@*h*-SiO_2 are more physically and chemically stable than bulk Ag_3PO_4 as evident from the low silver release from Ag_3PO_4@*h*-SiO_2. Hence, Ag_3PO_4@*h*-SiO_2 presents obvious visible-light induced

photocatalytic disinfection activity, largely surpassing *h*-SiO_2 and bulk Ag_3PO_4. These disinfection results match well with the superior photocatalytic MB degradation ability of Ag_3PO_4@*h*-SiO_2. It has been documented that the disinfectant activity of Ag-based NPs is size-dependent, and smaller particles always present higher disinfection efficiency when an equivalent amount of silver mass is used as small particles size gives a large surface area to volume ratios [12, 35]. Our results reveal that Ag_3PO_4@*h*-SiO_2 exhibits higher stability with much lower silver release than bulk Ag_3PO_4. That result can be ascribed to the presence of functional thiols on *h*-SiO_2 surface, which makes Ag_3PO_4 NPs more stable [21, 36]. The high chemical and physical stability without obvious silver leaching is an environmental-friendly and economic outcome of using Ag_3PO_4@*h*-SiO_2 as a potential photocatalytic disinfectant for water and wastewater treatment. Most importantly, minimization of silver release does not sacrifice the overall disinfection performance of Ag_3PO_4@*h*-SiO_2 due to the high surface areas of incorporated Ag_3PO_4. Therefore, the disinfection performance of hierarchical Ag_3PO_4@*h*-SiO_2 under visible-light irradiation is dominated by its enhanced photo-disinfection activity.

The above experimental findings were further confirmed by another qualitative disinfection tests using the Kirby–Bauer method [18]. Similarly, comparable dosages of NPs (4.25 mg/ml *h*-SiO_2, 0.75 mg/ml Ag_3PO_4 and 5.00 mg/ml Ag_3PO_4@*h*-SiO_2) were used based on their contents in Ag_3PO_4@*h*-SiO_2. Figure 6 indicates that tests with buffer solution only and *h*-SiO_2 do not show obvious inhibition zones under both dark and visible-light irradiation. Those results agree well with those disinfection activities in liquid medium. Bulk Ag_3PO_4 exhibits a more obvious inhibition zone with diameter of 8 mm than that of Ag_3PO_4@*h*-SiO_2 in dark, confirming its higher silver release from bulk Ag_3PO_4. Superior photocatalytic disinfection performance of Ag_3PO_4@*h*-SiO_2 under visible-light irradiation can be confirmed by a noticeable inhibition zone (13 mm), which is much larger than that of bulk Ag_3PO_4.

To further investigate the role of Ag_3PO_4@*h*-SiO_2 during the photo-disinfection process, morphological change in *E. coli* was studied by SEM before (Fig. 6c-d) and after (Fig. 6e-f) exposing the pathogen strain to Ag_3PO_4@*h*-SiO_2 suspensions under visible-light radiation. The pristine *E. coli* strain exhibits a well-defined IB structure and an evenly distributed interior content, indicating the structural integrity of bacteria [35]. However, after exposure to Ag_3PO_4@*h*-SiO_2 and 50 min visible-light irradiation, *E. coli* are severely damaged and show a typical shape with collapsed outer membrane and indented surface, confirming the superior photo-disinfection activity of Ag_3PO_4@*h*-SiO_2.

Analysis on photo-disinfection mechanism

From the above evaluation, the excellent photocatalytic disinfection ability of Ag_3PO_4@*h*-SiO_2 is associated with its chemical and structure advantages. Based on energy levels, a plausible mechanism diagram is depicted in Fig. 7a. Under visible-light irradiation, the photo-excited electrons in nanostructured Ag_3PO_4 jump from its valence band (VB) to conduction band (CB) (Eq. 1) [37–39], whereas the left holes can be trapped by OH^- or H_2O to generate reactive oxidant species such as OH· and H_2O_2 (Eqs. 2–4) [27],40. In addition, the accumulated photo-excited electrons in the CB involve a multiple-electron reduction reaction with O_2 to yield H_2O_2 (Eq. 5) [18, 41, 42].

$$Ag_3O_4 + hv \rightarrow e^- + h^+ \quad (1)$$

$$H_2O + h^+ \rightarrow H^+ + \bullet OH \quad (2)$$

$$OH^- + h^+ \rightarrow \bullet OH \quad (3)$$

$$\bullet OH + \bullet OH \rightarrow H_2O_2 \quad (4)$$

$$O_2 + 2H^+ + 2e^- \rightarrow H_2O_2 \quad (5)$$

For the visible-light irradiated Ag_3PO_4@*h*-SiO_2 aqueous system, H_2O_2, OH· and photo-generated holes are potential reactive species for pathogen disinfection [43]. To further understand detailed Ag_3PO_4@*h*-SiO_2 disinfection mechanism, various quenching experiments were conducted by introducing different scavengers of 2-propanol, Cr (VI), EDTA and Fe (II). 2-propanol is an OH· quencher to suppress OH·-mediated reactions [43]. The formation of OH· radical can be further confirmed by photoluminescence technique (**Figure S5**). EDTA is a scavenger for photo-generated holes [39]. Cr (VI) can capture photo-excited electrons to eliminate H_2O_2 generation (Eqs. 4 and 5) [44]. Fe (II) enhances OH· generation through the Fenton reaction [45].

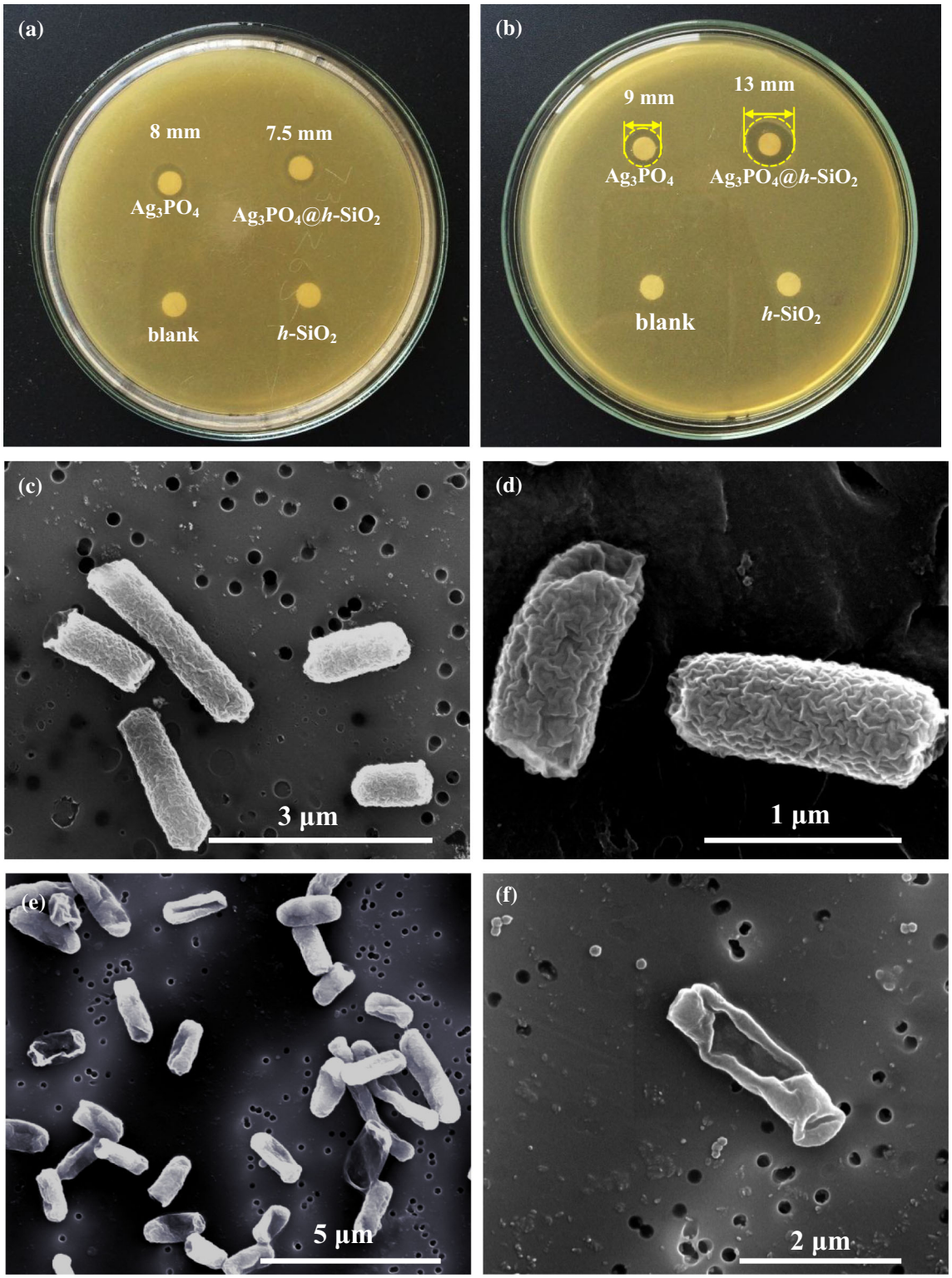

Figure 6 Inhibition zone plates in dark **a** and under visible light irradiation for 10 min **b** for sterilized buffer solution (blank), 0.0425 mg h-SiO_2 NPs, 0.0075 mg Ag_3PO_4 NPs and 0.05 mg Ag_3PO_4@*h*-SiO_2; SEM images of *E. coli* before **c** and after **e** been disinfected by Ag_3PO_4@*h*-SiO_2 under visible-light irradiation.

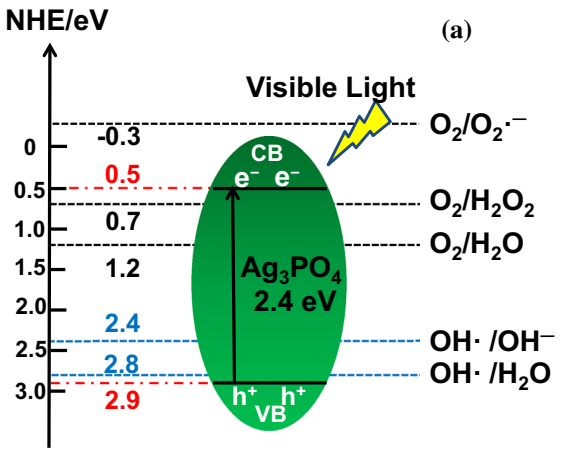

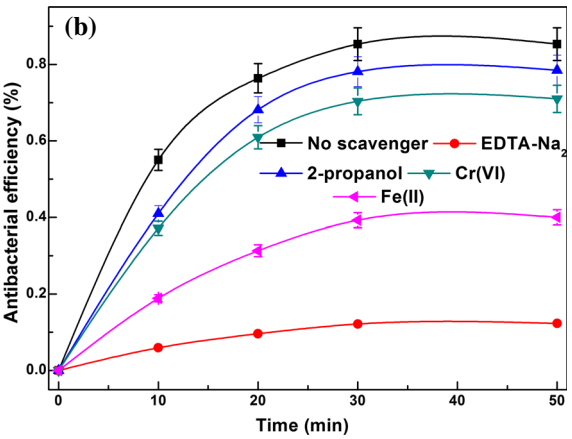

Figure 7 **a** Schematic diagram showing the photocatalytic disinfection mechanism against *E. coli*; **b** Effect of different scavengers (0.5 mM EDTA-Na_2, 0.05 mM Cr(VI), 0.5 mM 2-propanol and 0.1 mM Fe(II)) on photocatalytic disinfection efficiencies against *E. coli* (10^9 CFU/ml, 20 mL) using Ag_3PO_4@*h*-SiO_2 under visible-light irradiation.

Figure 7b compares the time-dependent photo-disinfection of *E. coli* exposure to Ag_3PO_4@*h*-SiO_2 and visible-light irradiation with and without scavengers. The disinfection efficiency decreases slightly after adding 2-propanol as an OH· scavenger, implying OH· is involved in the photo-disinfection but not dominative [46]. More drop of photo-disinfection efficiency after introducing Cr (VI) as an e^- scavenger suggests the H_2O_2 generated via the multiple-electron reduction reaction with O_2 near the CB of Ag_3PO_4 (Eq. 5) also contribute the disinfection process. However, the addition of Fe (II) as a H_2O_2 scavenger leads to obvious decrease on photo-disinfection efficiency, indicating H_2O_2 plays a large part in the disinfection process. Through the Fenton reaction with H_2O_2, Fe (II) introduction promotes OH· generation [43] but the obvious reduction on photo-disinfection after adding of Fe (II) in this study confirms the important role of H_2O_2 rather than OH·. In addition, the disinfection efficiency greatly drops when introducing EDTA as a quencher of photo-generated holes, indicating holes play a major role in this photo-disinfection process because of their intrinsic oxidative ability. Therefore, h^+ and H_2O_2 are dominative reactive species for photocatalytic disinfection in the presence of Ag_3PO_4@*h*-SiO_2 [47].

Conclusion

Novel high-efficient photocatalyst of Ag_3PO_4@*h*-SiO_2 was synthesized through a facile in situ precipitation method to anchor 10 nm Ag_3PO_4 NPs to the large pores of surface modified hierarchical porous SiO_2. The special and unique structure of Ag_3PO_4@*h*-SiO_2 leads to its outstanding photocatalytic activities towards pathogen disinfection and organic degradation. Quantitative disinfection evaluation in liquid and disk diffusion assays reveal that Ag_3PO_4@*h*-SiO_2 has outstanding photocatalytic oxidation activities under visible-light irradiation associated with its good chemical and physical stability, enhanced Ag_3PO_4 specific areas and eliminated silver release. Different from other silver-based disinfection systems, the photo-generated reactive species dominate the enhanced photo-disinfection efficiency of Ag_3PO_4@*h*-SiO_2. Detailed mechanism analysis through scavenger study proves that the photo-generated holes and H_2O_2 are mainly responsible for the photocatalytic activities of Ag_3PO_4@*h*-SiO_2. This high-performance and environmental-friendly photocatalyst can be used for both organic degradation and pathogen removal in water or wastewater treatment systems.

Acknowledgements

This work is financially supported by the Australian Research Council (DP160104632) and Scientific Research Program of Baoji University of Arts and Sciences (No 209010962).

Compliance with ethical standards

Conflict of interest The authors declare no conflict of interest.

Supplementary information: The online version of this article (https://doi.org/10.1007/s10853-021-05852-y)

References

[1] Matsunaga T, Tomoda R, Nakajima T, Wake H (1985) Photoelectrochemical sterilization of microbial cells by semiconductor powders. FEMS Microbiol Lett 29(1–2):211–214. https://doi.org/10.1111/j.1574-6968.1985.tb00864.x

[2] Ma S, Zhan S, Jia Y, Shi Q, Zhou Q (2016) Enhanced disinfection application of Ag-modified gC_3N_4 composite under visible light. Appl Catal B 186:77–87. https://doi.org/10.1016/j.apcatb.2015.12.051

[3] Yang X, Qin J, Jiang Y, Chen K, Yan X, Zhang D, Li R, Tang H (2015) Fabrication of P25/Ag_3PO_4/graphene oxide heterostructures for enhanced solar photocatalytic degradation of organic pollutants and bacteria. Appl Catal B 166:231–240. https://doi.org/10.1016/j.apcatb.2014.11.028

[4] Applerot G, Lipovsky A, Dror R, Perkas N, Nitzan Y, Lubart R, Gedanken A (2009) Enhanced antibacterial activity of nanocrystalline ZnO due to increased ROS-mediated cell injury. Adv Funct Mater 19(6):842–852. https://doi.org/10.1002/adfm.200801081

[5] Deng C-H, Gong J-L, Zeng G-M, Jiang Y, Zhang C, Liu H-Y, Huan S-Y (2016) Graphene–CdS nanocomposite inactivation performance toward Escherichia coli in the presence of humic acid under visible light irradiation. Chem Eng J 284:41–53. https://doi.org/10.1016/j.cej.2015.08.106

[6] Li G, Zhai J, Li D, Fang X, Jiang H, Dong Q, Wang E (2010) One-pot synthesis of monodispersed ZnS nanospheres with high antibacterial activity. J Mater Chem 20(41):9215–9219. https://doi.org/10.1039/C0JM01776K

[7] Sun B, Chen Y, Tao L, Zhao H, Zhou G, Xia Y, Wang H, Zhao Y (2018) Nanorod array of SnO_2 quantum dot interspersed multiphase TiO_2 heterojunctions with highly photocatalytic water splitting and self-rechargeable battery-like applications. ACS Appl Mater Inter 11(2):2071–2081. https://doi.org/10.1021/acsami.8b18884

[8] Liu L, Liu J, Sun DD (2012) Graphene oxide enwrapped Ag_3PO_4 composite: towards a highly efficient and stable visible-light-induced photocatalyst for water purification. Catal Sci Technol 2(12):2525–2532. https://doi.org/10.1039/C2CY20483E

[9] Yi Z, Ye J, Kikugawa N, Kako T, Ouyang S, Stuart-Williams H, Yang H, Cao J, Luo W, Li Z (2010) An orthophosphate semiconductor with photooxidation properties under visible-light irradiation. Nat Mater 9(7):559–564. https://doi.org/10.1038/nmat2780

[10] Agnihotri S, Mukherji S, Mukherji S (2013) Immobilized silver nanoparticles enhance contact killing and show highest efficacy: elucidation of the mechanism of bactericidal action of silver. Nanoscale 5(16):7328–7340. https://doi.org/10.1039/C3NR00024A

[11] Kim YH, Lee DK, Cha HG, Kim CW, Kang YS (2007) Synthesis and characterization of antibacterial Ag-SiO_2 nanocomposite. J Phys Chem C 111(9):3629–3635. https://doi.org/10.1021/jp068302w

[12] Buckley JJ, Lee AF, Olivi L, Wilson K (2010) Hydroxyapatite supported antibacterial Ag_3PO_4 nanoparticles. J Mater Chem 20(37):8056–8063. https://doi.org/10.1039/C0JM01500H

[13] Yang X, Cui H, Li Y, Qin J, Zhang R, Tang H (2013) Fabrication of Ag_3PO_4-graphene composites with highly efficient and stable visible light photocatalytic performance. Acs Catal 3(3):363–369. https://doi.org/10.1021/cs3008126

[14] Saint-Cricq P, Wang J, Sugawara-Narutaki A, Shimojima A, Okubo T (2013) A new synthesis of well-dispersed, core–shell Ag@SiO_2 mesoporous nanoparticles using amino acids and sugars. J Mater Chem B 1(19):2451. https://doi.org/10.1039/c3tb20210k

[15] Sharma M, Ojha K, Ganguly A, Ganguli AK (2015) Ag_3PO_4 nanoparticle decorated on SiO_2 spheres for efficient visible light photocatalysis. New J Chem 39(12):9242–9248. https://doi.org/10.1039/C5NJ01157D

[16] Yan Y, Zhou X, Li M, Li X, Kang X, Liu X, Huoa X, Huang G (2014) Ag_3PO_4 photocatalysts loaded on uniform SiO_2 supports for efficient degradation of methyl orange under

visible light irradiation. RSC Adv 4:5. https://doi.org/10.1039/C4RA06135G

[17] Hong X, Li M, Shan S, Hui K, Mo M, Yuan X (2016) Chloride ion-driven transformation from Ag_3PO_4 to AgCl on the hydroxyapatite support and its dual antibacterial effect against Escherichia coli under visible light irradiation. Environ Sci Pollut Res 23:13458–13466. https://doi.org/10.1007/s11356-016-6530-7

[18] Zheng P, Zhang B, Jin B, Guan W, Bai B, Dai S (2018) Synergistic Enhancement in Antibacterial Activity of Core/Shell/Shell SiO_2/ZnO/Ag_3PO_4 Nanoparticles. ChemNanoMat 4:972–981. https://doi.org/10.1002/cnma.201800195

[19] Zhang K, Xu L-L, Jiang J-G, Calin N, Lam K-F, Zhang S-J, Wu H-H, Wu G-D, Bl A, Bonneviot L (2013) Facile large-scale synthesis of monodisperse mesoporous silica nanospheres with tunable pore structure. J Am Chem Soc 135(7):2427–2430. https://doi.org/10.1021/ja3116873

[20] Xiong L, Du X, Shi B, Bi J, Kleitz F, Qiao SZ (2015) Tunable stellate mesoporous silica nanoparticles for intracellular drug delivery. J Mater Chem B 3(8):1712–1721. https://doi.org/10.1039/C4TB01601G

[21] Park J-h, Park J-k, Shin H-y (2007) The preparation of Ag/mesoporous silica by direct silver reduction and Ag/functionalized mesoporous silica by in situ formation of adsorbed silver. Mater Lett 61(1):156–159. https://doi.org/10.1016/j.matlet.2006.04.118

[22] Yao YR, Huang WZ, Zhou H, Cui X, Zheng YF, Song XC (2014) Synthesis of core–shell nanostructured magnetic photocatalyst Fe_3O_4@ SiO_2@ Ag_3PO_4 with excellent visible-light-responding photocatalytic activity. J Nanopart Res 16(11):1–10. https://doi.org/10.1007/s11051-014-2742-2

[23] Du X, Shi B, Liang J, Bi J, Dai S, Qiao SZ (2013) Developing functionalized dendrimer-like silica nanoparticles with hierarchical pores as advanced delivery nanocarriers. Adv Mater 25(41):5981–5985. https://doi.org/10.1002/adma.201302189

[24] Liu L, Tang Y, Dai S, Kleitz F, Qiao SZ (2016) Smart surface-enhanced Raman scattering traceable drug delivery systems. Nanoscale 8:12803–12811. https://doi.org/10.1039/C6NR03869G

[25] Xiong L, Du X, Kleitz F, Qiao SZ (2015) Cancer-Cell-Specific Nuclear-targeted drug delivery by dual-ligand-modified mesoporous silica nanoparticles. Small 11(44):5919–5926. https://doi.org/10.1002/smll.201501056

[26] Wang W-S, Du H, Wang R-X, Wen T, Xu A-W (2013) Heterostructured Ag_3PO_4/AgBr/Ag plasmonic photocatalyst with enhanced photocatalytic activity and stability under visible light. Nanoscale 5(8):3315–3321. https://doi.org/10.1039/C3NR00191A

[27] Xu J-W, Gao Z-D, Han K, Liu Y, Song Y-Y (2014) Synthesis of magnetically separable Ag_3PO_4/TiO_2/Fe_3O_4 heterostructure with enhanced photocatalytic performance under visible light for photoinactivation of bacteria. ACS Appl Mater Inter 6(17):15122–15131. https://doi.org/10.1021/am5032727

[28] Ebert D, Bhushan B (2012) Transparent, superhydrophobic, and wear-resistant coatings on glass and polymer substrates using SiO_2, ZnO, and ITO nanoparticles. Langmuir 28(31):11391–11399. https://doi.org/10.1021/la301479c

[29] Landskron K, Ozin GA (2004) Periodic mesoporous dendrisilicas. Science 306(5701):1529–1532. https://doi.org/10.1126/science.1104555

[30] Adams LK, Lyon DY, Alvarez PJ (2006) Comparative eco-toxicity of nanoscale TiO_2, SiO_2, and ZnO water suspensions. Water Res 40(19):3527–3532. https://doi.org/10.1016/j.watres.2006.08.004

[31] Liu J-K, Luo C-X, Wang J-D, Yang X-H, Zhong X-H (2012) Controlled synthesis of silver phosphate crystals with high photocatalytic activity and bacteriostatic activity. CrystEngComm 14(24):8714–8721. https://doi.org/10.1039/C2CE25604E

[32] Sotiriou GA, Pratsinis SE (2010) Antibacterial activity of nanosilver ions and particles. Environ Sci Technol 44(14):5649–5654. https://doi.org/10.1021/es101072s

[33] Bi Y, Ouyang S, Umezawa N, Cao J, Ye J (2011) Facet effect of single-crystalline Ag_3PO_4 sub-microcrystals on photocatalytic properties. J Am Chem Soc 133(17):6490–6492. https://doi.org/10.1021/ja2002132

[34] Wu A, Tian C, Chang W, Hong Y, Zhang Q, Qu Y, Fu H (2013) Morphology-controlled synthesis of Ag_3PO_4 nano/microcrystals and their antibacterial properties. Mater Res Bull 48(9):3043–3048. https://doi.org/10.1016/j.materresbull.2013.04.054

[35] Pang M, Hu J, Zeng HC (2010) Synthesis, morphological control, and antibacterial properties of hollow/solid Ag_2S/Ag heterodimers. J Am Chem Soc 132(31):10771–10785. https://doi.org/10.1021/ja102105q

[36] Ladhe A, Frailie P, Hua D, Darsillo M, Bhattacharyya D (2009) Thiol-functionalized silica–mixed matrix membranes for silver capture from aqueous solutions: experimental results and modeling. J Membr Sci 326(2):460–471. https://doi.org/10.1016/j.memsci.2008.10.025

[37] Yang Z-M, Huang G-F, Huang W-Q, Wei J-M, Yan X-G, Liu Y-Y, Jiao C, Wan Z, Pan A (2014) Novel Ag_3PO_4/CeO_2 composite with high efficiency and stability for photocatalytic applications. J Mater Chem A 2(6):1750–1756. https://doi.org/10.1039/C3TA14286H

[38] Guan X, Guo L (2014) Cocatalytic effect of $SrTiO_3$ on Ag_3PO_4 toward enhanced photocatalytic water oxidation.

Acs Catal 4(9):3020–3026. https://doi.org/10.1021/cs5005079

[39] Eswar NK, Katkar VV, Ramamurthy PC, Madras G (2015) Novel AgBr/Ag_3PO_4 decorated ceria nanoflake composites for enhanced photocatalytic activity toward dyes and bacteria under visible light. Ind Eng Chem Res 54(33):8031–8042. https://doi.org/10.1021/acs.iecr.5b01993

[40] Wang W, Zhang L, An T, Li G, Yip H-Y, Wong P-K (2011) Comparative study of visible-light-driven photocatalytic mechanisms of dye decolorization and bacterial disinfection by B-Ni-codoped TiO_2 microspheres: the role of different reactive species. Appl Catal, B 108:108–116. https://doi.org/10.1016/j.apcatb.2011.08.015

[41] Bi Y, Hu H, Ouyang S, Jiao Z, Lu G, Ye J (2012) Selective growth of Ag_3PO_4 submicro-cubes on Ag nanowires to fabricate necklace-like heterostructures for photocatalytic applications. J Mater Chem 22(30):14847–14850. https://doi.org/10.1039/C2JM32800C

[42] Rawal SB, Do Sung S, Lee WI (2012) Novel Ag_3PO_4/TiO_2 composites for efficient decomposition of gaseous 2-propanol under visible-light irradiation. Catal Commun 17:131–135. https://doi.org/10.1016/j.catcom.2011.10.034

[43] Zhang L-S, Wong K-H, Yip H-Y, Hu C, Yu JC, Chan C-Y, Wong P-K (2010) Effective photocatalytic disinfection of *E. coli* K-12 using AgBr−Ag−Bi2WO6 nanojunction system irradiated by visible light: the role of diffusing hydroxyl radicals. Environ Sci Technol 44(4):1392–1398. https://doi.org/10.1021/es903087w

[44] Wang W, Yu JC, Xia D, Wong PK, Li Y (2013) Graphene and g-C_3N_4 nanosheets cowrapped elemental α-sulfur as a novel metal-free heterojunction photocatalyst for bacterial inactivation under visible-light. Environ Sci Technol 47(15):8724–8732. https://doi.org/10.1021/es4013504

[45] Jia Y, Zhan S, Ma S, Zhou Q (2016) Fabrication of TiO2–Bi2WO6 binanosheet for enhanced solar photocatalytic disinfection of *E. coli*: insights on the mechanism. ACS Appl Mater Inter 8(11):6841–6851. https://doi.org/10.1021/acsami.6b00004

[46] Wang W, Ng TW, Ho WK, Huang J, Liang S, An T, Li G, Jimmy CY, Wong PK (2013) $CdIn_2S_4$ microsphere as an efficient visible-light-driven photocatalyst for bacterial inactivation: synthesis, characterizations and photocatalytic inactivation mechanisms. Appl Catal, B 129:482–490. https://doi.org/10.1016/j.apcatb.2012.09.054

[47] Wang W, Cheng B, Yu J, Liu G, Fan W (2012) Visible-light photocatalytic activity and deactivation mechanism of Ag3PO4 spherical particles. Chem Asian J 7(8):1902–1908. https://doi.org/10.1002/asia.201200197